SYSTEMATIC NUCLEAR STRUCTURE AND NUCLEAR REACTION STUDIES RELEVANT TO p-PROCESS

Awanish Bajpeyi, A. Shukla

Department of Physics, Rajiv Gandhi Institute of Petroleum Technology
Jais, Amethi, India

A.J. Koning

Nuclear Physics and Nuclear Data Evaluation, International Atomic Energy Agency, Austria
and
Department of Physics and Astronomy, Applied Nuclear Physics
Uppsala University, Uppsala, Sweden

(Received July 11, 2017; accepted November 28, 2017)

The cross section and reaction rate of the proton and alpha capture reactions on ^{102}Pd, ^{120}Te, ^{124,126}Xe, and ^{130,132}Ba have been calculated through TALYS in Hauser–Feshbach formalism using relativistic mean field densities. Nuclear structure studies have been also carried out for the nuclei under consideration. Results obtained in the present work for nuclear structure as well as nuclear reaction are in a fair agreement with the available experimental results.

DOI:10.5506/APhysPolB.49.27

1. Introduction

The nuclear landscape that defines the nuclear physics territory is quite interesting for number of reasons. On the one hand, it motivates exhaustive research efforts to stretch the existing limits of nuclear existence and determine the endpoints of dripline by experimentally producing new elements, on the other hand, it poses serious challenges to our understanding — to explain the formation, as well as the abundance of some of the existing nuclei, lying on the proton rich side of the stability valley, though well within the limits of nuclear landscape. Currently, it contains approximately four thousand isotopes of elements, which are basic building blocks for the universe, having about three hundred isotopes stable and remaining others unstable [1]. Production of these stable as well as unstable isotopes is understood through the nucleosynthesis process, which involves number of nuclear reactions. Production of nuclei lying up to iron mainly proceeds by H burning, He burning, CNO cycle, α, e, and few other processes, and the abundance of the nuclei up to iron can be reasonably explained through the reaction networks formed by these nuclei. Any further formation of nuclei heavier than iron is expected to involve additional reaction processes, proposed firstly by Burbidge *et al.* and Cameron, where subsequent β decay and neutron capture processes [2, 3] play major role. These neutron capture processes are characterized by two different mechanisms: the rapid neutron capture process, by which synthesis of approximately half of the nuclei are formed heavier than iron, occurs in highly explosive stellar environment leading to the formation of r-nuclides, those located on the neutron rich side of valley of nuclear stability, and the process is known as r-process. The other process is slow neutron capture process, which happens in stellar helium and carbon burning environment leading to the formation of s-nuclides, those situated at the bottom of the valley of nuclear stability and the process is commonly termed as s-process. The neutron capture s- and r-processes are responsible for the formation of bulk of heavy elements. However, the series of these processes leaves about thirty five nuclei between ^{74}Se to ^{196}Hg, blocked by neutron capture, s- and r-processes. These nuclei are expected to be formed by the p-process and are called p-nuclei [2].

The p-nuclei are much less abundant (except for ^{92,94}Mo and ^{96,98}Ru) in comparison to other nuclei, heavier than iron, which are formed by neutron capture, r- and s-processes [4, 5]. The possible sites and scenarios responsible for p-process are still under discussion, though it is largely agreed that p-process proceeds through a large network of photo-disintegration reactions, such as (γ, n), (γ, p), (γ, α) and potential sites for the p-process are the explosively burning Ne/O shells in the shock-heated envelopes of type II supernova explosions where a pre-existing s/r-seed distribution is eroded by photon-induced reactions at temperatures between 2–3 GK [6–9]. There have been limited experimental attempts employing different techniques to measure relevant cross sections using activation method, in-beam methods (angular distributions method and γ-summing technique), γ-induced reactions and techniques in inverse kinematics with varying projectile energy range [10–14].

Although experimental cross sections data provide key information to calculate the abundance of the p-nuclei, yet such experimental observations are scarce because of two major limitations for performing these experiments. Firstly, in the laboratory target, nucleus is always in its ground state, while target nucleus lies in thermally excited state under stellar conditions and secondly, in the case of heavy nuclei, high nuclear level density and high Coulomb barriers also make the experimental efforts quite challenging. Moreover, typical p-process reaction network calculation involves nearly two thousand nuclei and approximately twenty thousand reactions, and most of the nuclei involved in this reaction network are unstable. Thus, it is very difficult to perform a large number of experiments in laboratory and to understand the p-process nucleosynthesis solely through experimental measurements. Thus, theoretical considerations are genuinely required to supplement experimental studies and provide input for the network calculations to meet the shortfall of cross-sections data. Even if experimental cross-section data are available, very often these data are not fully commensurable with the energy regime of the stellar situation. In such cases, cross sections obtained with theoretical models can be normalized to the available experimental data. If the uncertainty of the energy dependence of the calculated cross section is small, this method provides a safe extrapolation to the relevant stellar energies from the measured energies.

In the theoretical framework, reaction cross-section results are obtained by the Hauser–Feshbach [15] statistical model calculations and this cross section is used to calculate the astrophysical reaction rates, which is further required for p-process network studies based on theoretical models [16]. The parameters *i.e* nuclear level density, optical potential, γ-ray strength function, and nuclear masses enter as an input for the calculation of cross sections with the statistical model code. The theoretical calculations depend on the reliability of these inputs and hence the uncertainty in calculated cross-section results depend on the uncertainties of these inputs. Therefore, it is highly desired to ensure the reliability of model inputs by calculating as many experimental observables as possible and compare with the experimental observations. Statistical model codes *e.g.* MOST [17], SMARAGD [18, 19], NON-SMOKER [20–22] and TALYS [23] have been used widely for the nuclear reaction calculations. TALYS code covers most of the major reaction mechanisms which are important for light particle induced nuclear reactions *i.e.* direct, pre-equilibrium, and compound mechanisms to calculate the total reaction probability, and the code is optimized for large projectile energy range from 1 keV to 200 MeV [23, 24].

In the present work, we have calculated the cross section and reaction rate for proton and alpha capture reactions for ^{102}Pd, ^{120}Te, ^{124,126}Xe, and ^{130,132}Ba in the Hauser–Feshbach statistical model (using TALYS 1.6), using microscopic and phenomenological optical potential obtained using densities calculated from the relativistic mean field (RMF) approach. The assessment of the reliability of the nuclear densities, used as an input for reaction studies, has been performed by comparing ground state properties of the nuclei *i.e.* binding energy, r.m.s. matter radii, and r.m.s. radii, calculated by RMF model [25] with the corresponding experimental observations. We have used microscopic optical model potential (JLM) [26] and phenomenological optical model potential (KD03) [27] for the nuclear reaction calculations. In the microscopic optical model, the nucleon–nucleon effective interaction is folded with the matter density distribution to quantify the strength and shape of the nuclear potential, while in the case of phenomenological optical model, the Woods–Saxon form has been taken into account for the determination of depth and parametrization has been used to best fit with existing experimental data. The paper is presented in the following manner. The mathematical formalism is described in Section 2. The results are presented and discussed along with the comparison with theoretical as well as experimental existing results in Section 3. At last, conclusion and summary are given in Section 4.

2. Mathematical formalism

The reaction cross section $\sigma^{\mu\nu}(E_{ij})$ of reaction $i^{\mu}(j,o)m^{\nu}$ from the target state i^{μ} to the excited state m^{ν} of the final nucleus can be written as

$$\begin{aligned}\sigma^{\mu\nu}(E_{ij}) &= \frac{\pi\hbar^2/(2\mu_{ij}E_{ij})}{(2J_i^{\mu}+1)(2J_j+1)}\sum_{J,\pi}(2J+1)\\ &\quad\times\frac{T_j^{\mu}\left(E,J,\pi,E_i^{\mu},J_i^{\mu},\pi_i^{\mu}\right)T_o^{\mu}\left(E,J,\pi,E_{m,}^{\nu}J_m^{\nu},\pi_m^{\nu}\right)}{T_{\mathrm{tot}}(E,J,\pi)}\,, \qquad (1)\end{aligned}$$

where E_{ij} denotes the excitation energy, J denotes the spin, and π is the parity of excited states. The $T_{\mathrm{tot}} = \sum_{\nu,o} T_o^{\nu}$ describes the transitions to all possible bound and unbound states ν in all energetically accessible exit channels o including the entrance channel i. Again, in this case, the contribution of the thermally excited states has to be estimated. The necessary energy E_{ij} for the tunneling is independent of the excitation energy, and hence the contribution of the excited states to the reaction cross section and reaction cross-section rate is much smaller in comparison to the (γ,p) reactions.

The cross sections are used to determine the stellar reaction rates (which are required for stellar evolution models to determine the formation of heavy nuclei), and can be written as

$$\langle\sigma v\rangle = \left(\frac{8}{\pi\mu}\right)^{1/2}\frac{N_{\mathrm{A}}}{(KT)^{3/2}}\int\limits_0^{\infty}\sigma^{\mu\nu}(E_{ij})E\exp\left(\frac{-E}{KT}\right)\mathrm{d}E\,, \qquad (2)$$

where N_{A} is the Avogadro number, KT is the thermal energy and E is the centre-of-mass energy. Another important task is to find the effective energy range for the cross sections to be calculated for the proton and alpha capture reactions. Following equations ((3) and (4)) are used to determine a relevant energy range $E_0 - \mathit{\Delta}/2 \leq E \leq E_0 + \mathit{\Delta}/2$ within which the nuclear cross sections have to be known [28]

$$E_0 = 0.12204\left(\mu_A {Z_1}^2 {Z_2}^2 {T_9}^2\right)^{1/3}\,, \qquad (3)$$

$$\mathit{\Delta} = 0.23682\left(\mu_A {Z_1}^2 {Z_2}^2 {T_9}^5\right)^{1/6}\,, \qquad (4)$$

where E_0, Δ are in the units of MeV, T_9 is the plasma temperature in GK, and $\mu = A_1A_2/(A_1 + A_2)$ is the reduced mass. The statistical model needs optical potential for reaction cross-section calculation, which further requires nuclear densities as input. In this work, relativistic mean field densities have been used as RMF is proved to be one of the most successful approaches among the existing mean field theories. In the relativistic mean field model, the nuclear many-body system is understood in terms of interacting particles baryons and mesons through mean field. The parameters of the model are phenomenologically fitted in accordance to the saturation properties of nuclear matter [29, 30]. RMF theory explains well salient features of finite nuclei such as binding energy of ground states, various excited states, deformation, charge radii, density profile and nuclear halo, *etc.* In the last three decades, the RMF model has been successfully used to explain the properties of finite nuclei as well as infinite nuclear matter [31–34]. One of the major attractive features of the RMF formalism is that the spin-orbit strength, other associated spin properties and associated nuclear shell structure automatically arise from meson–nucleon interaction [35, 36].

The details of RMF model and solving the equations for finite nuclei and nuclear matter can be found in the literature [33, 37–39]. The basic ingredient is the relativistic Lagrangian density for a nucleon–meson many-body system [33, 39]

$$\begin{aligned}\mathcal{L} \;=\; & \bar{\psi}_i\{i\gamma^\mu\partial_\mu - M\}\psi_i + \frac{1}{2}\partial^\mu\sigma\partial_\mu\sigma - \frac{1}{2}m_\sigma^2\sigma^2 - \frac{1}{3}g_2\sigma^3 - \frac{1}{4}g_3\sigma^4 - g_s\bar{\psi}_i\psi_i\sigma \\ & -\frac{1}{4}\Omega^{\mu\nu}\Omega_{\mu\nu} + \frac{1}{2}m_w^2V^\mu V_\mu + \frac{1}{4}c_3(V_\mu V^\mu)^2 - g_w\bar{\psi}_i\gamma^\mu\psi_i V_\mu - \frac{1}{4}B^{\mu\nu}B_{\mu\nu} \\ & +\frac{1}{2}m_\rho^2R^\mu R_\mu - g_\rho\bar{\psi}_i\gamma^\mu\tau\psi_i R^\mu - \frac{1}{4}F^{\mu\nu}F_{\mu\nu} - e\bar{\psi}_i\gamma^\mu\frac{(1-\tau_{3i})}{2}\psi_i A_\mu\,. \end{aligned} \tag{5}$$

The field for the σ meson is denoted by σ, that for the ω meson by V_μ and for the isovector ρ meson by R_μ. A^μ denotes the electromagnetic field. The ψ_i are the Dirac spinors for the nucleons whose third component of isospin is denoted by τ_{3i}. Here, g_s, g_w, g_ρ, and $\frac{e^2}{4\pi} = \frac{1}{137}$ are the coupling constants for σ, ω, ρ mesons and photon, respectively. g_2, g_3, and c_3 are the parameters for the nonlinear terms of σ and ω mesons. M is the mass of the nucleon and m_σ, m_ω and m_ρ are the masses of the σ, ω, and ρ mesons, respectively. $\Omega^{\mu\nu}$, $B^{\mu\nu}$ and $F^{\mu\nu}$ are the field tensors for the V^μ, R^μ and the photon fields, respectively [39].

3. Results and discussion

There are a number of parameter sets available for solving standard RMF Lagarangians, but in this work, we have used NL3* [40] parameter set as it has been found to study nuclear observable across the nuclear landscape in different nuclear mass region. The nuclear structure for the nuclei considered in the present work has been studied as a benchmark test to check the nuclear model reliability regarding shape and density. For this, we have calculated binding energy and r.m.s. charge radii of all the nuclei under consideration. Further, we have used relativistic mean field densities to calculate the JLM potential which is required as an input for calculating nuclear cross section and reaction rates.

3.1. Ground state properties — nuclear densities, binding energy, and r.m.s. charge radii

In Table I, we have presented the calculated ground state properties *i.e.* binding energy and r.m.s. charge radii for all nuclei under consideration along with the experimentally observed values. The root mean square (r.m.s.) charge radius (r_{c}) is obtained from the point proton r.m.s. radius through the relation given below [33]

$$r_{\mathrm{c}} = \sqrt{r_p^2 + 0.64}\,, \tag{6}$$

TABLE I

Comparison of calculated ground state properties of nuclei under consideration with the data available. The experimental values for B.E./A are taken from [41] and for $\mathrm{r_c}$ are taken from [42].

Nucleus	B.E./A (in MeV)		$\mathrm{r_c}$ (in fm)	
	RMF	EXPT.	RMF	EXPT.
^{102}Pd	−8.564	−8.580	4.475	4.482
^{120}Te	−8.456	−8.477	4.734	4.703
^{124}Xe	−8.421	−8.437	4.760	4.762
^{126}Xe	−8.431	−8.443	4.765	4.770
^{130}Ba	−8.396	−8.405	4.820	4.828
^{132}Ba	−8.402	−8.409	4.823	4.830
^{103}Ag	−8.540	−8.537	4.492	4.503
^{121}I	−8.436	−8.441	4.752	—
^{125}Cs	−8.398	−8.399	4.788	4.788
^{127}Cs	−8.412	−8.411	4.791	4.793
^{131}La	−8.373	−8.370	4.843	—
^{133}La	−8.382	−8.378	4.845	—
^{106}Cd	−8.524	−8.539	4.528	4.534
^{128}Ba	−8.386	−8.396	4.816	4.826
^{134}Ce	−8.336	−8.366	4.852	—
^{136}Ce	−8.370	−8.373	4.868	4.873

considering the size of proton radius as 0.8 fm. One can see from the results given in the table that our calculated results agree well with the experimental results. It is important to mention here that, since the charge radius $r_{\rm c}$ matches excellently with experimental results, therefore, one can reliably comment on the density profiles as well as density-dependent properties calculated using RMF densities which are employed to calculate the optical potential, for reaction cross-section calculations.

3.2. Cross section and reaction rate

The cross section and reaction rates have been calculated using two different optical potential *i.e.* KD03 potential and microscopic JLM potential through TALYS code using RMF densities. As discussed in previous section, these nuclear densities were separately calculated using RMF formalism and were added to TALYS source files manually for calculating the potential and further the cross section were calculated at astrophysically relevant energy windows. We have compared these reaction cross-section calculations with the available experimental data. The cross-section results have been plotted in the energy range of 2.5–6 MeV for proton capture and 9.5–14.5 MeV for the alpha capture reaction, and for reaction rate results temperature range 2 to 5 GK for proton capture and 4.5 to 7.5 GK for alpha capture reaction relevant to the Gamow Window. The results are displayed in Figs. 1–4, where we have shown the results of our calculations and compared with experimentally as well as theoretically available data.

Comparison of proton capture cross section and alpha capture cross section (as a function of energy in centre-of-mass frame) is presented (for ^{102}Pd, ^{120}Te, ^{124,126}Xe,^{130,132}Ba) in Figs. 1 and 2 respectively. In all the figures, calculated results with JLM potential and KD03 potential are showed using solid lines and dotted lines respectively. Dashed lines represent NON-SMOKER results and experimental data points with error bars are also shown. Comparison of proton capture rates and alpha capture rates (as a function of temperature) for these nuclei is given in Figs. 3 and 4 respectively. Cross section and reaction rate results (experimental) for $^{102}\mathrm{Pd}(p,\gamma)^{103}\mathrm{Ag}$ have been taken from Ozkan *et al.* [43]. In this experiment, an activation technique was used in which gamma rays from decays of reaction products were detected off-line by two hyper-pure germanium detectors in a low background environment. Experimental data for the cross section of $^{120}\mathrm{Te}(p,\gamma)^{121}\mathrm{I}$ is taken from Guray *et al.* [44]. In this experiment, an activation technique was used and the cross section were deduced from the observed gamma-ray activity, which was detected off-line by two clover HPGe detectors mounted in close geometry. Experimental results of cross section for $^{124}\mathrm{Xe}(\alpha,\gamma)^{128}\mathrm{Ba}$ have been taken from Halász *et al.* [45]. In this experiment, cross sections was measured with the activation technique us-

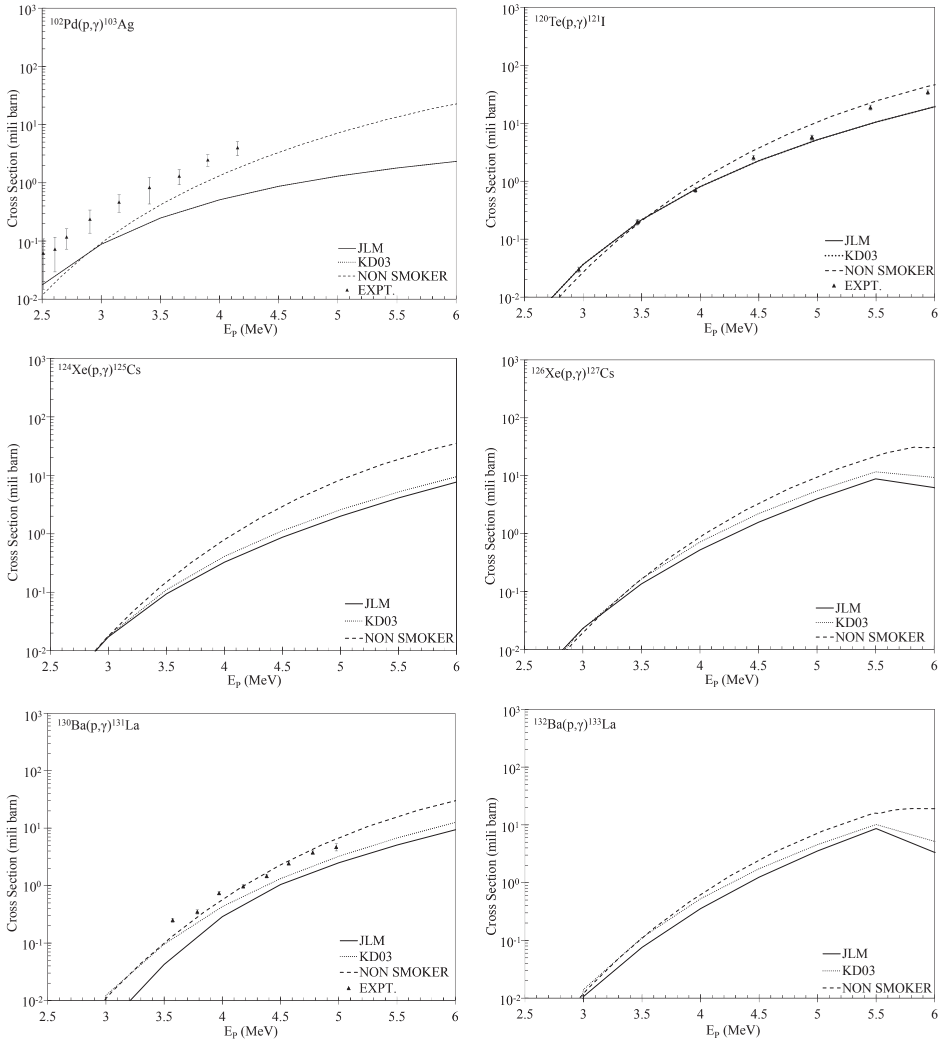

Fig. 1. Comparison of proton capture cross section for ^{102}Pd, ^{120}Te, ^{124}Xe, and ^{130}Ba (as a function of energy in centre-of-mass frame).

ing a thin window ^{124}Xe gas cell. Cross-section results (experimental) for $^{130}\mathrm{Ba}(p,\gamma)^{131}\mathrm{La}$ are taken from Netterdon *et al.* [46]. In this experimental work, cross-section values were measured by the activation technique. After the irradiation with protons, the reaction yield was determined by the use of gamma-ray spectroscopy using two clover-type high-purity germanium detectors. Experimental data for $^{130}\mathrm{Ba}(\alpha,\gamma)^{134}\mathrm{Ce}$ was obtained using the activation technique with HPGe detector [47]. In the case of $^{102}\mathrm{Pd}(\alpha,\gamma)^{104}\mathrm{Cd}$, $^{120}\mathrm{Te}(\alpha,\gamma)^{124}\mathrm{Xe}$, $^{124}\mathrm{Xe}(p,\gamma)^{125}\mathrm{Cs}$, $^{126}\mathrm{Xe}(p,\gamma)^{127}\mathrm{Cs}$, and $^{126}\mathrm{Xe}(\alpha,\gamma)^{130}\mathrm{Ba}$,

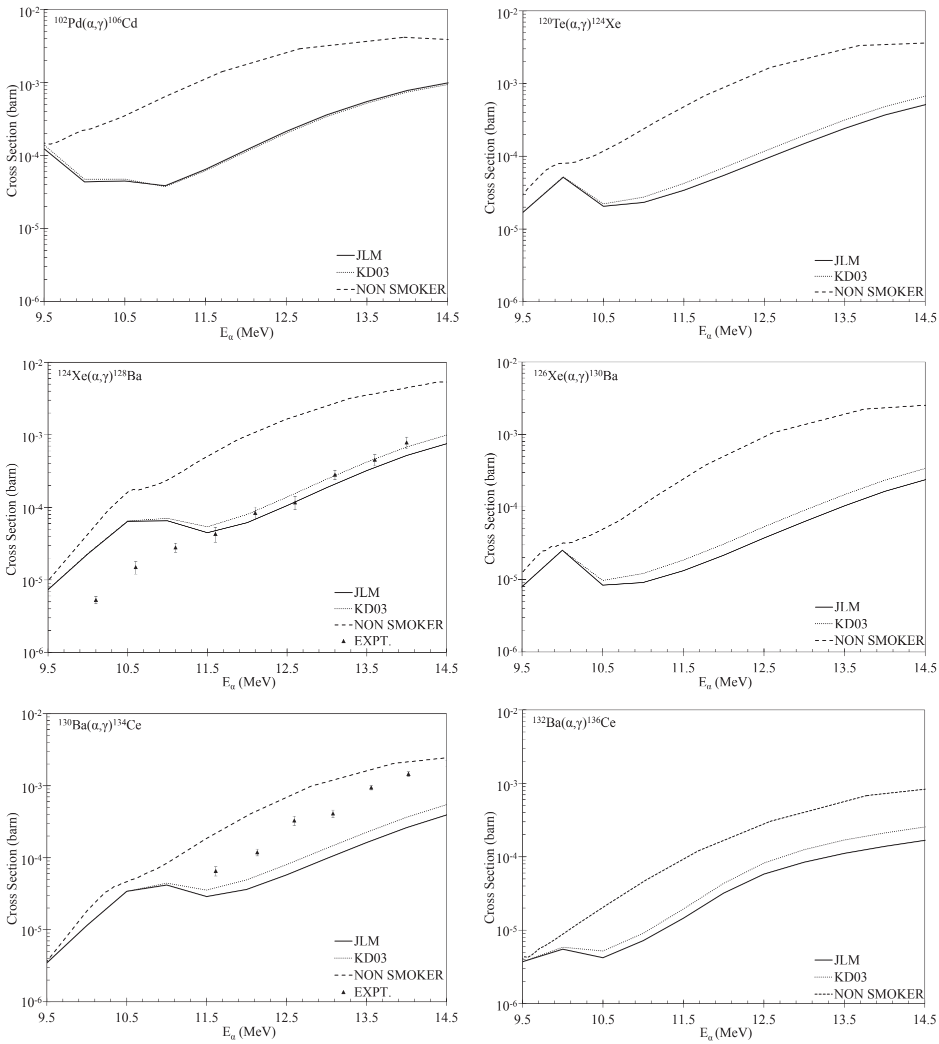

Fig. 2. Comparison of alpha capture cross section for ^{102}Pd, ^{120}Te, ^{124}Xe, and ^{130}Ba (as a function of energy in centre-of-mass frame).

$^{132}\mathrm{Ba}(p,\gamma)^{133}$La and $^{132}\mathrm{Ba}(\alpha,\gamma)^{136}$Ce, no experimental results are available, hence the calculated results are given as prediction and are also compared with the other theoretical results (NON-SMOKER).

One can see from the results displayed that our results obtained through JLM as well as KD03 potential are quite similar in nature, qualitatively as well as quantitatively but show some difference from NON-SMOKER results, and the present work approach can describe the experimental results in a few cases. One can also see that the difference between JLM, KD03 and NON-

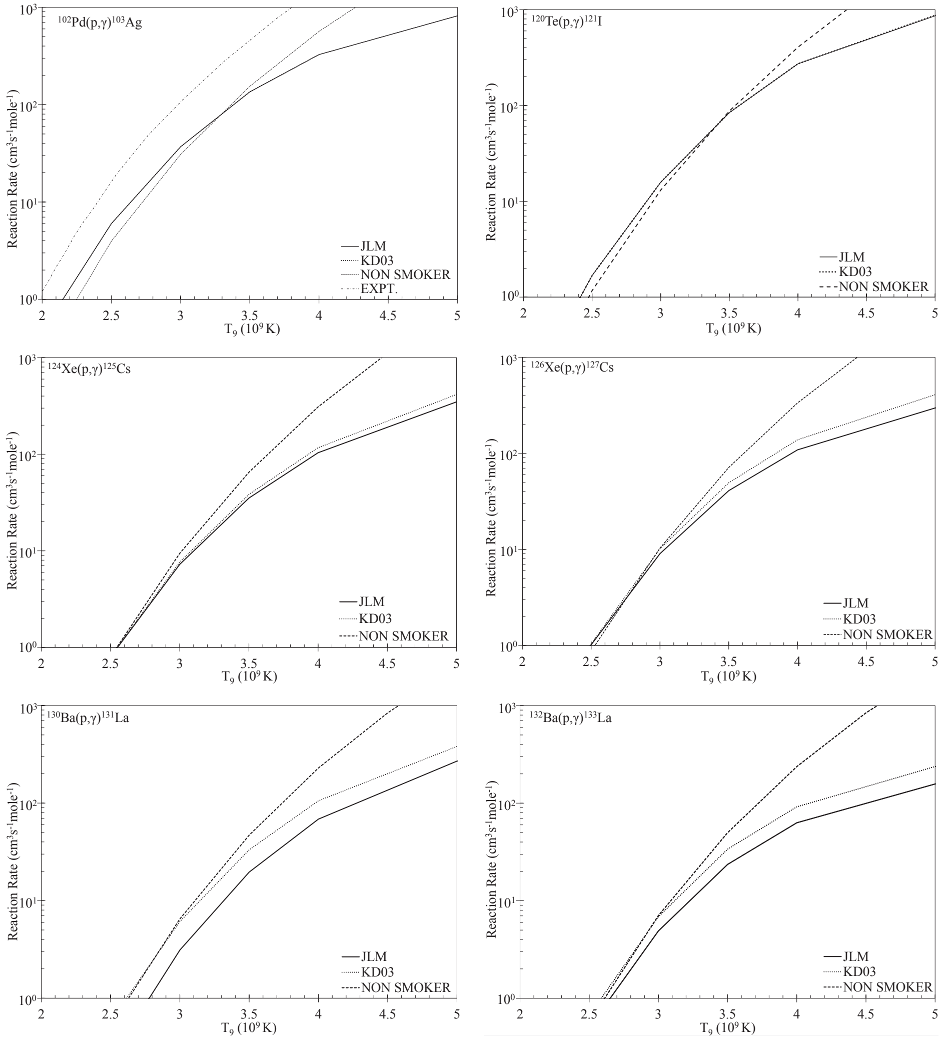

Fig. 3. Comparison of proton capture rates for ^{102}Pd, ^{120}Te, ^{124,126}Xe, and ^{130,132}Ba (as a function of temperature).

SMOKER results are small at lower energy/temperature ranges but becomes considerable for the higher energy/temperature ranges. Cross-section results for proton capture reactions displayed in Fig. 1 and our predictions are very close to experimental results with only exception of $^{102}\mathrm{Pd}(p,\gamma)^{103}\mathrm{Ag}$ result. For the case of $^{124}\mathrm{Xe}(p,\gamma)^{125}\mathrm{Cs}$, $^{126}\mathrm{Xe}(p,\gamma)^{127}\mathrm{Cs}$ and $^{132}\mathrm{Ba}(p,\gamma)^{133}\mathrm{La}$, due to unavailability of experimental results, they are displayed only with existing theoretical predictions. We find that our results have similar trend with the NON-SMOKER results. The alpha capture cross-section results are plot-

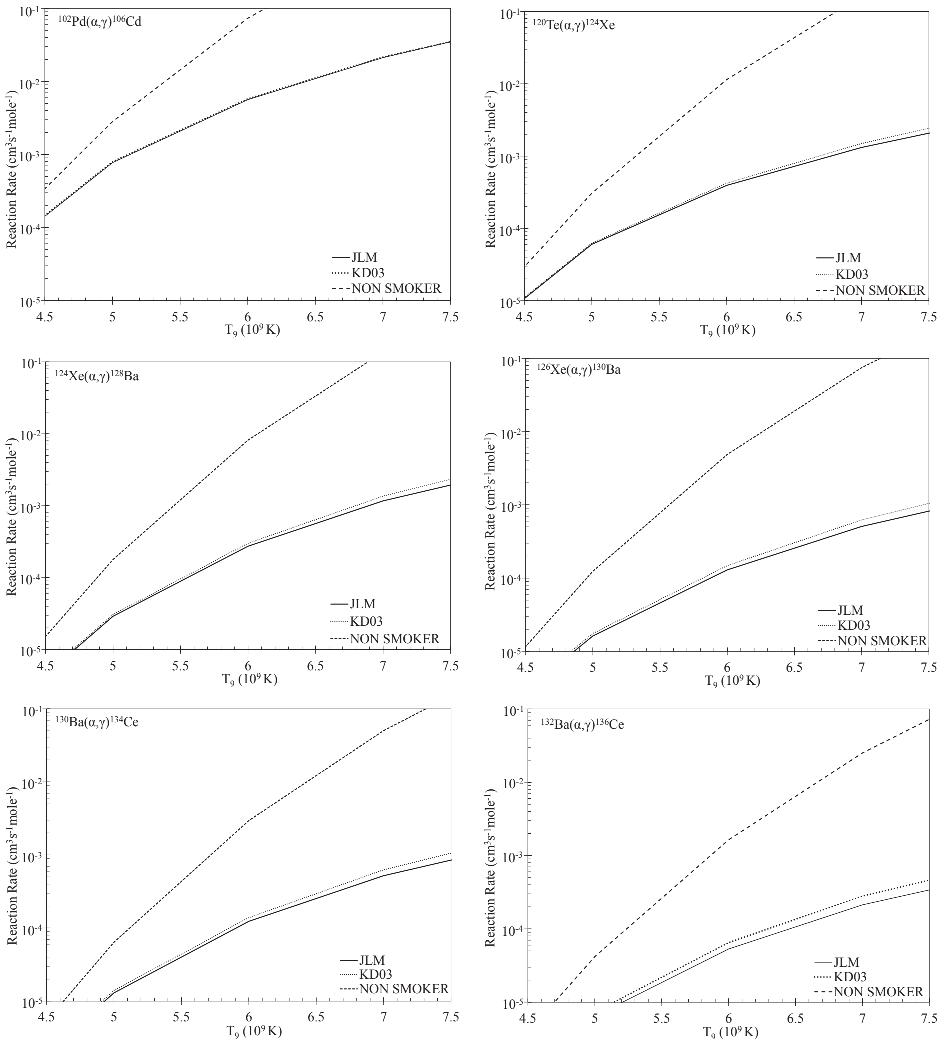

Fig. 4. Comparison of alpha capture rates for ^{102}Pd, ^{120}Te, ^{124,126}Xe, and ^{130,132}Ba (as a function of temperature).

ted in Fig. 2 and only for $^{124}\mathrm{Xe}(\alpha,\gamma)^{128}\mathrm{Ba}$ and $^{130}\mathrm{Ba}(\alpha,\gamma)^{134}\mathrm{Ce}$ reactions experimental results are available, for other cases, we compared our predictions only with available theoretical results. In the case of $^{124}\mathrm{Xe}(\alpha,\gamma)^{128}\mathrm{Ba}$ reaction, JLM and KD03 results perfectly match with the experimental results, while the NON-SMOKER results are larger by a factor of 2–3 than our results. Moreover, our results for cross section are in a good agreement with the existing experimental results except for $^{102}\mathrm{Pd}(p,\gamma)^{103}\mathrm{Ag}$ and $^{130}\mathrm{Ba}(\alpha,\gamma)^{134}\mathrm{Ce}$ cross-section results. We have also compared the NON-

SMOKER astrophysical reaction rate results with our calculations for the proton and alpha capture reactions (graphed in Figs. 3 and 4) considered in the present work to see how much extent present work reaction rates differ from the preexisting results. Only the experimental reaction rate for ^{102}Pd$(p,\gamma)^{103}$Ag is available, which has been shown in Fig. 3. We find that our reaction rate results are smaller than the astrophysical rates calculated using NON-SMOKER formalism by a factor of 1–3 approximately.

Considering this comparative analysis, it can be said that the present work for the cross section and reaction rate calculations provide reasonable results to explain experimental data, however, these results need to be further improved to have better agreement with the experimental results. Also, it could be worthwhile to see the effect of nuclear level density in such reaction studies along with the study of more astrophysical reactions, involving stable as well as unstable nuclei. Specifically, this kind of approach to study nuclear structure and reactions in coherent manner, involving microscopic nuclear inputs certainly opens up an avenue for reducing the uncertainty in theoretical tools being adopted for calculating nuclear reaction cross sections, to be further used for reaction network calculations.

4. Conclusion

In the present work, nuclear structure and reaction studies have been performed for the p-nuclei under consideration. The nuclear structure observables have been calculated by relativistic mean field model (RMF) and the results have been found to be in the excellent agreement with the experimental results. This can be taken as a measure of reliability for using these RMF densities for the calculation of cross section and reaction rate with microscopic and phenomenological optical potential using nuclear reaction code (TALYS). The calculated cross sections and reaction rates results are found to be in a good agreement with the experimental results as well as theoretical (NON-SMOKER) results. As reaction network for the nucleosynthesis of heavy nuclei requires the reaction cross sections and reaction rates data, in bulk, at high temperature so the present study will be helpful to fulfill this need. The aim of our study is to perform more reliable nuclear reaction calculations, which are coherent with nuclear structure studies as well. Such approach will help reducing the uncertainty in theoretical calculations and will limit the number of models and parameter sets available for explaining plethora of nuclear observables across the nuclear landscape. Most importantly, such studies are necessary to better understand the formation and abundance of p-nuclei.

One of the authors (A.S.) is highly thankful for the research grant provided by DST (DST Reference No. SB/FTP/PS-004/2013) to carry out this work.

REFERENCES

[1] J. Magill, G. Pfennig, R. Dreher, Z. Sóti: Karlsruher Nuklidkarte/Chart of the Nuclides, 9$^{\rm th}$edition, Nucleonica GmbH, Eggenstein–Leopoldshafen, 2015.

[2] E.M. Burbidge, G.R. Burbidge, W.A. Fowler, F. Hoyle, *Rev. Mod. Phys.* **29**, 547 (1957).

[3] A.G.W. Cameron, Chalk River Rep. CRL, Atomic Energy Can. Ltd., 41, 1957.

[4] T. Rauscher *et al.*, *Rep. Prog. Phys.* **76**, 066201 (2013).

[5] A. Bajpeyi, A.J. Koning, A. Shukla, S. Åberg, *Eur. Phys. J. A* **51**, 157 (2015).

[6] R. Reifarth, C. Lederer, F. Kappeler, *J. Phys. G: Nucl. Part. Phys.* **41**, 053101 (2014).

[7] C. Travaglio, F.K.R. Opke, R. Gallino, W. Hillebrandt, *Astrophys. J.* **739**, 2 (2011).

[8] M. Rayet *et al.*, *Astron. Astrophys.* **298**, 517 (1995).

[9] D.L. Lambert, *Astron. Astrophys. Rev.* **3**, 201 (1992).

[10] W. Rapp *et al.*, *Phys. Rev. C* **78**, 025804 (2008).

[11] K. Vogt *et al.*, *Phys. Rev. C* **63**, 055802 (2001).

[12] A. Simon *et al.*, *Phys. Rev. C* **87**, 055802 (2013).

[13] I. Precup *et al.*, *Rom. Rep. Phys.* **64**, 64 (2012).

[14] O. Ershova *et al.*, *PoS* **NICXI**, 232 (2010).

[15] W. Hauser, H. Feshbach, *Phys. Rev.* **87**, 366 (1952).

[16] P. Mohr, *AIP Conf. Proc.* **704**, 532 (2004).

[17] S. Goriely, *IOP Conf. Ser.* **529**, 287 (2000); `http://www-astro.ulb.ac.be/Html/hfr.html`

[18] T. Rauscher, *Int. J. Mod. Phys. E* **20**, 1071 (2011).

[19] T. Rauscher, code SMARAGD, version 0.8.3s, 2011.

[20] T. Rauscher, F.K. Thielemann, *At. Data Nucl. Data Tables* **75**, 1 (2000).

[21] T. Rauscher, F.K. Thielemann, *At. Data Nucl. Data Tables* **79**, 1 (2001).

[22] `http://nucastro.org/nonsmoker.html`

[23] A.J. Koning, S. Hilaire, M.C. Duijvestijn, TALYS-1.0, Proceedings of the International Conference on Nuclear Data for Science and Technology — ND2007, April 22–27, 2007, Nice, France, eds. O. Bersillon *et al.*, EDP Sciences, 2008, p. 211.

[24] A. Bajpeyi, A. Shukla, A.J. Koning, S. Åberg, *Phys. At. Nucl.* **80**, 402 (2017).

[25] P. Ring, Y.K. Gambhir, G.A. Lalazisis, *Comput. Phys. Commun.* **105**, 77 (1997).

[26] J.P. Jeukenne, A. Lejeune, C. Mahaux, *Phys. Rev. C* **16**, 80 (1977).

[27] A.J. Koning, J. Delaroche, *Nucl. Phys. A* **713**, 231 (2003).

[28] T. Rauscher, *Phys. Rev. C* **81**, 045807 (2010).

[29] P. Ring, *Prog. Part. Nucl. Phys.* **37**, 193 (1996).

[30] P.G. Reinhard, *Rep. Prog. Phys.* **52**, 439 (1989).

[31] A. Shukla, S. Åberg, S.K. Patra, *J. Phys. G: Nucl. Part. Phys.* **38**, 095103 (2011).

[32] R. Machleidt, *Adv. Nucl. Phys.* **19**, 189 (1989).

[33] S.K. Patra, C.R. Praharaj, *Phys. Rev. C* **44**, 2552 (1991).

[34] M.D. Estal, M. Centelles, X. Viñas, S.K. Patra, *Phys. Rev. C* **63**, 024314 (2001).

[35] C.J. Horowitz, B.D. Serot, *Nucl. Phys. A* **368**, 503 (1981).

[36] B.D. Serot, J.D. Walecka, *Adv. Nucl. Phys.* **16**, 1 (1986).

[37] M. Rufa *et al.*, *Phys. Rev. C* **38**, 390 (1988).

[38] P.G. Reinhard, *Z. Phys. A* **329**, 257 (1988).

[39] Y.K. Gambhir, P. Ring, A. Thimet, *Ann. Phys.* **198**, 132 (1990).

[40] G.A. Lalazissis *et al.*, *Phys. Lett. B* **36**, 671 (2009).

[41] `http://www.nndc.bnl.gov/masses/`

[42] I. Angeli, *At. Data Nucl. Data Tables* **87**, 185 (2004).

[43] N. Özkan *et al.*, *Nucl. Phys. A* **688**, 459 (2001).

[44] R.T. Güray *et al.*, *Phys. Rev. C* **80**, 035804 (2009).

[45] Z. Halász *et al.*, *Phys. Rev. C* **94**, 045801 (2016).

[46] L. Netterdon *et al.*, *Phys. Rev. C* **90**, 035806 (2014).

[47] Z. Halász *et al.*, *Phys. Rev. C* **85**, 025804 (2012).